JOURNAL OF GUIDANCE, CONTROL, AND DYNAMICS
Vol. 31, No. 3, May–June 2008

Indirect Optimization of Two-Dimensional Finite Burning Interplanetary Transfers Including Spiral Dynamics

Christopher L. Ranieri* and Cesar A. Ocampo†
University of Texas at Austin, Austin, Texas 78712

DOI: 10.2514/1.30833

Using methods previously developed for accurately estimating the unknown costates for escape and capture spirals, the indirect optimization problem for a two-dimensional simplification of the low-Earth-orbit to low-Mars-orbit transfer is solved. The goal of the optimization is to compute minimum propellant trajectories for finite burning engines. Solutions are considered with and without control limits on specific impulse and compared with previous research. A regimented step-by-step process is developed that facilitates the construction of low-Earth-orbit to low-Mars-orbit missions in two dimensions. In direct comparison with past research, more fuel-efficient trajectories are found with the same mission objectives and constraints. The iterative approach used in this other research to reduce the final Martian orbit from 300 to 6 Mars radii (20,382 km) is removed in favor of a more direct approach. The new approach allows a much greater range of functionality because solutions are found with much lower final Martian circular orbits of 1.32–1.77 Mars radii (4500–6000 km).

Nomenclature

a	=	thrust acceleration magnitude
$\mathbf{e}_*$	=	unit vector for coordinate frames (* is the axis subscript)
G	=	Bolza function
H	=	Hamiltonian
J	=	cost function
m	=	spacecraft mass
P	=	spacecraft power
$\mathbf{R_s}$	=	position vector of the spacecraft from the sun
R_{Sr}, $R_{S\theta}$	=	position components of the $\mathbf{R_s}$ vector in the Earth frame
r, r'	=	polar position magnitude in the Earth–Mars frame
r_{mr}, $r_{m\theta}$	=	radial and tangential components of the $\mathbf{r}'$ position vector in the Earth frame
t	=	time
$\mathbf{u}$	=	thrust acceleration unit direction vector
V_{RS}, $V_{\theta S}$	=	inertial velocity components of the spacecraft in the heliocentric polar frame
V_{RSE}, $V_{\theta SE}$	=	inertial velocity components of the spacecraft in the Earth frame
V_{rE}, $V_{\theta E}$	=	polar velocity components of Earth around the sun
V_{rM}, $V_{\theta M}$	=	polar velocity components of Mars around the sun
v_r, v_θ	=	velocity components of the spacecraft in the Earth frame
$v_{r'}$, $v_{\theta'}$	=	velocity components of the spacecraft in the Mars frame
θ, θ'	=	polar angle in the Earth–Mars frame
$\dot{\theta}$	=	angular velocity of the polar angle
λ	=	costates
μ	=	gravitational parameter
ξ	=	temp angle rotating from Earth to Mars frames or vice versa
ψ	=	temp angle rotating from Earth or Mars frames to the heliocentric frame

Received 5 March 2007; revision received 3 November 2007; accepted for publication 5 November 2007.

*National Science Foundation Graduate Student, Department of Aerospace Engineering and Engineering Mechanics, 1 University Station, Mail Stop C0600; chris.ranieri@gmail.com. Member AIAA.

†Associate Professor, Department of Aerospace Engineering and Engineering Mechanics, 1 University Station, Mail Stop C0600; cesar.ocampo@mail.utexas.edu. Member AIAA.

Introduction

AN INDIRECT optimization procedure is presented for optimizing the fuel usage for transfers for finite burning engines from low Earth orbit (LEO) to low Martian orbit (LMO). For this research, the solar system model is simplified, with Earth and Mars in circular two-dimensional orbits. The overall trajectory can be categorized by three sections: Earth-escape spiral, heliocentric transfer, and Mars-capture spiral. Analysis of the optimality conditions for the heliocentric legs, particularly for time-constrained round-trip missions, has previously been developed [1,2]. Additionally, in-depth analysis has been performed focusing solely on the escape and capture portions of such missions [3].

The engine model used is a variable-specific-impulse (VSI) engine in which the power is constant but the specific impulse or thrust magnitude can be throttled accordingly. Examples are also presented in which control limits are introduced for the I_{sp} in particular cases in which the I_{sp} is constrained to be a constant during the escape. The optimal control problem is solved as an indirect optimization problem; the associated Euler–Lagrange equations are integrated numerically. A boundary-value problem is then solved to optimize the trajectory. From this formulation, the values of the thrust acceleration magnitude and direction are determined to be continuous functions of the costates.

Although numerous papers exist on optimizing interplanetary missions that include the spiral dynamics with direct methods, analytical methods, and other approximate solutions, the research presented focuses on indirect methods. Other works have analyzed end-to-end LEO-to-LMO [4,5] or low-lunar-orbit (LLO) [6–9] missions using indirect methods. These works may simplify the engine dynamics, particularly during the most detailed phases of the trajectories, the spirals, by limiting the thrust to be constant [6–8] or, at the very least, by using a constant thrust spiral as the first guess [4,5]. Some papers use indirect optimization for analysis of a single phase of the full LEO-to-LMO mission, such as a spiral escape or capture, but do not link seamlessly with the heliocentric legs [3,10]. Others use indirect methods and analytical approximations of spiral orbit transfers for Earth-orbiting applications only [3,11]. Many papers just use a patched conic approach and calculate the spirals and heliocentric legs independently. These works do not optimize the spirals themselves, but rather calculate fixed constant-thrust spirals

with the thrust fixed along the velocity vector until the spacecraft achieves escape [12,13]. These spirals are then patched with a zero-sphere-of-planetary-influence heliocentric model. The goal of this research is to find optimal trajectories that are not dependent on such assumptions or simplifications of the problem dynamics. This paper will show the importance of the first guess in determining which local optimal solution is generated with respect to the global solution space. Most important, the process used is significantly different from the previous research on LEO–LMO missions [4,5].

Like past research [4,5], a series of subproblems must be optimized to construct the full mission. The full mission includes gravitational effects during the entire trajectory from all three major bodies of the problem: Earth, sun, and Mars. The main difference of the new approach is to analyze the entire trajectory in an Earth-referenced polar coordinate system rotating with spacecraft around the Earth (labeled as ECR) as the Earth revolves around the sun. To facilitate this approach, a transformation is derived to convert costates in a Mars-referenced polar frame rotating with the spacecraft around Mars (labeled as MCR) as Mars revolves around the sun to their equivalent costates in the ECR frame. This greatly simplifies the optimal control conditions that must be satisfied at the patch point. It also allows the problem to be solved as a multiple-shooting-method problem in which the Earth escape and heliocentric transfer are integrated forward and the Mars capture is separately integrated backward. These transformations and the regimented order of subproblems allows the analyst to find a broader range of missions to much lower LMOs than were previously achievable, as well as to find more fuel-efficient solutions for the exact mission scenarios previously published. This process heavily uses the techniques previously developed [3] for optimizing the spirals alone and uses the previously published works of Vadali et al. [4,5] as both a foundation for the method developed here (with the important differences clearly explained) and as a benchmarking resource.

Problem Definition

Equations of Motion

Noninertial coordinate frames (ECR and MCR) that track the motion of the planets with respect to the sun are used. These coordinate systems can be seen in Fig. 1, which depicts three polar coordinate systems referenced to the heliocentric inertial frame ($\mathbf{i_S}$, $\mathbf{j_S}$): Earth polar (e_{rE}, $e_{\theta E}$), Mars polar (e_{rM}, $e_{\theta M}$), and the spacecraft-centered Earth-position-referenced frame (ECR: e_r, e_θ). The coordinate axes for the MCR frame ($e_{r'}$, $e_{\theta'}$) are omitted from the diagram for the sake of clarity. The MCR frame has the $e_{r'}$ axis along the r' direction and the $e_{\theta'}$ axis along the appropriate counterclockwise tangential direction from the $e_{r'}$ axis. The planets and sun are denoted with their astrological symbols in Fig. 1. The equations of motion are developed under the assumption that Earth and Mars are in circular orbits.

Using the ECR coordinate system, the state and state time derivative are defined:

$$\mathbf{x} = \begin{bmatrix} r \\ \theta \\ v_r \\ v_\theta \end{bmatrix} \tag{1}$$

$$\dot{\mathbf{x}} = \begin{bmatrix} \dot{r} = v_r \\ \dot{\theta} = v_\theta / r \\ \dot{v}_r \\ \dot{v}_\theta \end{bmatrix} \tag{2}$$

The position of the spacecraft with respect to the sun can be written as

$$\mathbf{R_S} = \begin{bmatrix} R_E \cos\theta_E + r\cos(\theta + \theta_E) \\ R_E \sin\theta_E + r\sin(\theta + \theta_E) \end{bmatrix}_{(i_S, j_S)} = \begin{bmatrix} R_E \cos\theta + r \\ -R_E \sin\theta \end{bmatrix}_{(e_r, e_\theta)} = \begin{bmatrix} R_{Sr} \\ R_{S\theta} \end{bmatrix} \tag{3}$$

The position of the spacecraft with respect to Mars is

$$\mathbf{r}' = \begin{bmatrix} r_{mr} \\ r_{m\theta} \end{bmatrix}_{(e_r, e_\theta)} = \begin{bmatrix} r + R_E \cos\theta - R_M \cos(\theta + \theta_E - \theta_M) \\ R_M \sin(\theta + \theta_E - \theta_M) - R_E \sin\theta \end{bmatrix}_{(e_r, e_\theta)} \tag{4}$$

Using these definitions, the equations of motion in the ECR frame can be completed:

$$\begin{bmatrix} \dot{v}_r \\ \dot{v}_\theta \end{bmatrix} = \begin{bmatrix} -\mu_E / r^2 - \mu_S R_{Sr} / R_S^3 - \mu_M r_{mr} / r'^3 + (v_\theta + \dot{\theta}_E r)^2 / r + R_E \dot{\theta}_E^2 \cos\theta + a u_r \\ -\mu_S R_{S\theta} / R_S^3 - \mu_M r_{m\theta} / r'^3 - v_\theta v_r / r - 2 v_r \dot{\theta}_E - R_E \dot{\theta}_E^2 \sin\theta + a u_\theta \end{bmatrix} \tag{5}$$

where the angular velocity of the Earth is

$$\dot{\theta}_E = V_{\theta E} / R_E \tag{6}$$

The equivalent equations can be determined in the MCR frame with a few modifications.

Earth-to-Sun Transformation

From Fig. 1, the heliocentric polar position is

$$R_S = \sqrt{(R_E + r\cos\theta)^2 + (r\sin\theta)^2} \tag{7}$$

$$\theta_S = \theta_E + \tan^{-1}[r\sin\theta / (R_E + r\cos\theta)] \tag{8}$$

The inertial velocity of the spacecraft with respect to the sun, written in the ECR frame is

$$\begin{bmatrix} V_{RSE} \\ V_{\theta SE} \end{bmatrix} = \begin{bmatrix} v_r + R_E \dot{\theta}_E \sin\theta \\ v_\theta + \dot{\theta}_E (r + R_E \cos\theta) \end{bmatrix}_{(e_r, e_\theta)} \tag{9}$$

The inertial velocity of the spacecraft with respect to the sun in the heliocentric polar frame is

$$\begin{bmatrix} V_{RS} \\ V_{\theta S} \end{bmatrix}_{(e_{rS}, e_{\theta S})} = \begin{bmatrix} \cos\psi & \sin\psi \\ -\sin\psi & \cos\psi \end{bmatrix} \begin{bmatrix} V_{RSE} \\ V_{\theta SE} \end{bmatrix} \tag{10}$$

$$\psi = \theta_S - \theta_E - \theta \tag{11}$$

Equations (7), (8), and (10) give the spacecraft position and the inertial velocity with respect to the sun in the heliocentric polar

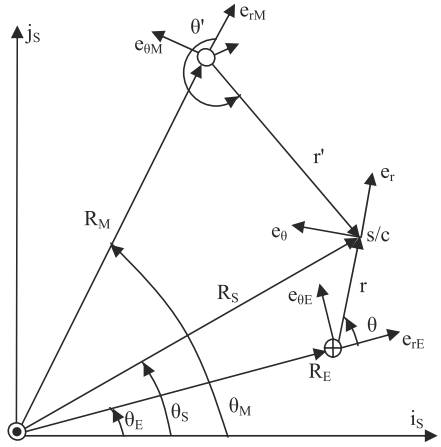

Fig. 1 Polar coordinate systems.

frame. This frame is not drawn in Fig. 1, for clarity. Its position-referenced axis e_{RS} is along the position vector $\mathbf{R_S}$, with the tangential axis $e_{\theta S}$ perpendicular to e_{RS} in the counterclockwise direction. The equivalent Mars-to-sun transformation is found by simply changing the E and M subscripts and using the primed states r', θ', $v_{r'}$, and $v_{\theta'}$ instead of r, θ, v_r, and v_θ.

Sun-to-Earth Transformation

From Fig. 1, the polar position around Earth is written in terms of the heliocentric polar position and the polar position of Earth around the sun:

$$r = \sqrt{R_S^2 + R_E^2 - 2R_S R_E \cos(\theta_S - \theta_E)} \tag{12}$$

$$\begin{aligned} &\theta = \sin^{-1}[R_S \sin(\theta_S - \theta_E)/r] \quad \text{if } R_S \geq R_E \\ &\theta = \pi - \sin^{-1}[R_S \sin(\theta_S - \theta_E)/r] \quad \text{if } R_S < R_E \end{aligned} \tag{13}$$

To determine the ECR velocity components, the terms of Eq. (9) must be substituted into Eq. (10) and the two equations of Eq. (10) must be solved simultaneously:

$$v_\theta = (V_{\theta S} + V_{RS} \tan\psi)\cos\psi - \dot{\theta}_E(r + R_E \cos\theta) - \dot{R}_E \sin\theta \tag{14}$$

$$\begin{aligned} v_r = {} & [V_{RS} - \sin\psi(v_\theta + \dot{\theta}_E(r + R_E\cos\theta) - \dot{R}_E \sin\theta)]/\cos\psi \\ & - R_E\dot{\theta}_E \sin\theta - \dot{R}_E \cos\theta \end{aligned} \tag{15}$$

The sun-to-Earth transformation can be converted to a sun-to-Mars transformation by changing the E and M subscripts and using the primed states r', θ', $v_{r'}$, and $v_{\theta'}$ instead of r, θ, v_r, and v_θ.

Optimal Control Problem

To minimize the spacecraft propellant for a VSI engine, it is possible to decouple the actual spacecraft mass and power from the problem, and a formulation for the minimum-fuel problem can be used based solely on the accumulated thrust acceleration [14]:

$$\frac{1}{m_f} - \frac{1}{m_0} = \frac{1}{2}\int_{t0}^{tf}\left(\frac{a^2}{P}\right)\mathrm{d}t \tag{16}$$

The optimal value for the power for an unconstrained VSI engine is the maximum power level and can be removed. Using optimal control theory, a boundary-value problem is formed that, when satisfied, meets all of the first-order conditions for optimality [15]. Because the problem is formulated as a maximization problem, the cost function used is

$$J = \max\left[-\frac{1}{2}\int_{t0}^{tf} a^2\,\mathrm{d}t\right] \tag{17}$$

Once the boundary-value problem has been solved to optimize the cost function laid out in Eq. (17), the final mass m_f in Eq. (16) can be found by specifying values for the vehicle power and initial mass value:

$$m_f = \frac{m_0 P_{\max}}{P_{\max} + J m_0} \tag{18}$$

All physical constraints of the optimization problem, such as specifying the targeted state vector of the spacecraft at the final time at Mars, are adjoined to the cost function via the Bolza function G [15]:

$$G = \boldsymbol{\omega}^T \begin{bmatrix} r(t_f) - r^* \\ \theta(t_f) - \theta^* \\ v_r(t_f) - v_r^* \\ v_\theta(t_f) - v_\theta^* \end{bmatrix} = \mathbf{0} \tag{19}$$

$$J' = G - \frac{1}{2}\int_{t0}^{tf} a^2\,\mathrm{d}t \tag{20}$$

The controls are the thrust acceleration magnitude a and its unit direction vector $\mathbf{u}$. Their optimal values are derived by finding the stationary point of the Hamiltonian with respect to the controls. The acceleration is aligned with the primer vector [16]:

$$H = \boldsymbol{\lambda}^T \dot{\mathbf{x}} - a^2/2 \tag{21}$$

$$u_r^2 + u_\theta^2 = 1 \tag{22}$$

$$\mathbf{u} = \boldsymbol{\lambda}_\mathbf{v}/\lambda_v \tag{23}$$

$$a = \lambda_v \tag{24}$$

Using the definition of the Hamiltonian, the costate equations can be found:

$$\dot{\boldsymbol{\lambda}} = -H_{\mathbf{x}}^T \tag{25}$$

$$\begin{aligned} \dot{\lambda}_r = {} & \lambda_\theta v_\theta/r^2 - \lambda_{vr}[3\mu_M r_{mr}^2/r'^5] - \lambda_{v\theta}[v_\theta v_r/r^2 + 3\mu_S R_{Sr}R_{S\theta}/R_S^5 \\ & + 3\mu_M r_{mr}r_{m\theta}/r'^5] - \lambda_{vr}[2\dot{\theta}_E(v_\theta + \dot{\theta}_E r)/r - (v_\theta + \dot{\theta}_E r)^2/r^2] \\ & - \lambda_{vr}[2\mu_E/r^3 - \mu_S/R_S^3 + 3\mu_S R_{Sr}^2/R_S^5 - \mu_M/r'^3] \end{aligned} \tag{26}$$

$$\begin{aligned} \dot{\lambda}_\theta = {} & -\lambda_{vr}[-R_E\dot{\theta}_E^2 \sin\theta - \mu_S R_{S\theta}/R_S^3] - \lambda_{vr}[3\mu_S r(R_{Sr}R_{S\theta})/R_S^5 \\ & - \mu_M r_{M\theta}/r'^3 + 3\mu_M r_{mr}r_{m\theta}r/r'^5] \\ & - \lambda_{v\theta}[-R_E\dot{\theta}_E^2\cos\theta + \mu_S(R_{Sr} - r)/R_S^3 + 3\mu_S r(r_{s\theta}^2)/R_S^5] \\ & - \lambda_{v\theta}[\mu_M(r_{mr} - r)/r'^3 + 3\mu_M r_{m\theta}^2 r/r'^5] \end{aligned} \tag{27}$$

$$\begin{bmatrix} \dot{\lambda}_{vr} \\ \dot{\lambda}_{v\theta} \end{bmatrix} = \begin{bmatrix} -\lambda_r + \lambda_{v\theta}(v_\theta/r - 2\dot{\theta}_E) \\ -\lambda_\theta/r - 2\lambda_{vr}(v_\theta + \theta_E r)/r + \lambda_{v\theta}v_r/r \end{bmatrix} \tag{28}$$

If bounds on the I_{sp} are considered, a different cost function should be used:

$$J = \max(m_f) \tag{29}$$

As derived previously [3], a first guess for a solution with I_{sp} bounds can be found by multiplying the converged costates for the

unconstrained optimal control problem of Eq. (17) by the scalar $m^2/P_{\max}$.

Subproblems for End-to-End Optimization

Using these equations of motion, the preceding transformations between different coordinate frames and the formulation of the optimal control problem, a rigorous step-by-step process shown in Fig. 2, was developed to formulate the optimal LEO–LMO missions. Steps 1a–3a are identical to steps 1b–3b except, the a set of steps involve forward (FWD) integration from the initial conditions in an Earth-referenced frame, whereas the b set involves backward (BWD) integration from the final targeted state in a Mars-referenced frame.

Step 1a/1b

The goal of the first subproblem is to find fuel-optimal escape and capture spirals in a polar frame referenced to an Earth-centered-inertial (ECI) coordinate system for the escape spirals or a Mars-centered-inertial (MCI) coordinate system for the capture spirals. Escape and capture is considered to be the point at which the spacecraft has zero energy relative to its central body. Only the central body is acting on the trajectory during these spirals. The major point of past research is that very accurate estimates of the unknown costates for these spirals can be found using curve fits [3]. For this work, curve fits for escape spirals from an initial circular orbit of 6700 km, as well as capture spirals to six Mars radii [one Mars distance unit (DU_M) is 3397 km] of 1.77 and 1.32 DU_M, are generated.

The choice of integrating the capture spirals backward in time from the final circular orbit is a departure from the technique used in past works on LEO–LMO missions [4,5]. In those works, the capture is integrated forward, with the final orbit iteratively decreased in size as far as possible (from 300 to 6 DU_M) before encountering convergence problems [4]. Integrating the capture backward incorporates an initial guess for a capture spiral that is more detailed, leading to solutions with captures that terminate in much lower Martian orbits (1.32–1.77 DU_M).

Step 2a/2b

Although the solutions for the spirals in step 1 do not include the gravity of other bodies such as the sun and Mars/Earth and are performed in an inertial frame, the third-body perturbations and effects of the rotation of the ECR or MCR frames do not significantly alter the trajectory or the optimal costates for the escape or capture spirals found in step 1. Therefore, the costates found from step 1 are the initial guess for spirals in the ECR or MCR frames. The optimality targets are the same as in step 1, except for the fact that the polar angle θ is no longer cyclical and its initial costate must be included in the initial guess vector. The corresponding new target is a final value of zero for the polar-angle costate.

Step 3a/3b

The goal of step 3 is to optimally transfer from LEO through an escape spiral, transition to heliocentric space and target the capture point of the capture spiral found in step 2b. It was found that integrating both the Earth escape and the heliocentric transfer continuously in the ECR frame is easier numerically, matching the findings of the previously published works [4,5]. The same costates used for the Earth spiral from previous steps are used as the first guess for the solution that spirals away from Earth starting from LEO, continuously through heliocentric space, and then targets a point near Mars with little difficulty in convergence. It is important to note that no heliocentric-only portions of the trajectory are ever analyzed. It was found during the research process that including a heliocentric-only portion just complicated the problem setup. Changing coordinate frames at any point in the trajectory introduces a discontinuity in the spacecraft state that is addressed via optimal control theory [15] by introducing a discontinuity into the Bolza function in Eq. (20). The optimality conditions derived from this discontinuity are quite cumbersome, and integrating both phases in the ECR frame skips this numerically difficult step. For step 3b, the trajectory is integrated solely in the MCR frame and targets the escape point found in step 2a.

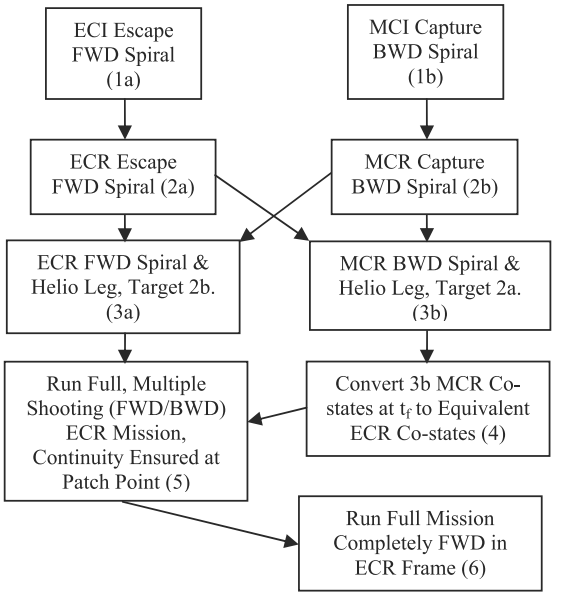

Fig. 2 Flow chart for subproblems for end-to-end optimization.

Step 4

This step is the most vital step for the increased performance shown in comparison with other published works. After step 3a, there are two ways to solve the full mission. The first way, used in previous works [4,5], integrates the capture forward and in the MCR frame. This is done after solving for the MCR costates at the start of the capture sequence in terms of the ECR costates by simultaneously solving the two optimal control conditions associated with the discontinuity [4,15]. Basically, the problem is set up as a single-shooting method. This approach is difficult. The forward-integration approach has to iteratively lower the final orbit to form the spiral and encounters convergence limits at relatively large final orbits (6 DU_M). Part of the numerical sensitivity is also associated with satisfying the conditions derived from the discontinuity at the patch point at which the state switches from ECR to MCR coordinates.

These difficulties can be avoided. Incorporating the backward capture spiral and heliocentric leg from step 3b that targets the Earth-escape point removes the need to iteratively lower the final orbit to form a spiral. This generates more involved capture sequences that terminate lower and have more revolutions around Mars. Another step involves a transformation that converts the MCR costates of step 3b to the equivalent ECR costates. This allows the entire LEO–LMO mission to be integrated solely in the ECR frame with no state discontinuities. These steps allow the problem to be formulated as a multiple-shooting-method in which the Earth-escape/heliocentric transfer and the Mars capture can be directly modified by the boundary-value solver used [17]. This added degree of freedom actually allows the boundary-value solver to more easily reach convergence. This setup allows it to adjust the two most difficult trajectory phases directly and independently, rather than indirectly adjusting the Martian capture sequence only through simultaneous adjustment of the Earth escape.

Earth Costates from Martian Costates Transformation

The theory behind this transformation was derived previously [3]. The main idea is that the thrust magnitude in both the MCR and ECR frames must be identical, and the thrust direction must point in the same inertial direction. Using this and the relationship between the velocity costates and thrust unit direction vector specified by Eqs. (23) and (24), the MCR velocity costates are converted to ECR velocity costates:

$$\xi = \theta + \theta_E - \theta_M - \theta' \tag{30}$$

$$\dot{\xi} = \dot{\theta} + \dot{\theta}_E - \dot{\theta}_M - \dot{\theta}' = v_\theta/r + V_{\theta E}/R_E - V_{\theta M}/R_M - v_{\theta'}/r' \tag{31}$$

$$\begin{bmatrix} \lambda_{vr} \\ \lambda_{v\theta} \end{bmatrix} = \begin{bmatrix} \cos\xi & \sin\xi \\ -\sin\xi & \cos\xi \end{bmatrix} \begin{bmatrix} \lambda_{vr'} \\ \lambda_{v\theta'} \end{bmatrix} \tag{32}$$

Taking the time derivative of Eq. (32) and inserting it in the appropriate costate equations for the ECR and MCR frames from Eq. (28), the final ECR costates are found:

$$\lambda_r = -\lambda_{v\theta}(v_\theta/r + 2\dot{\theta}_E) - \dot{\lambda}_{vr'}\cos\xi + \lambda_{vr'}\dot{\xi}\sin\xi - \dot{\lambda}_{v\theta'}\sin\xi - \lambda_{v\theta'}\dot{\xi}\cos\xi \tag{33}$$

$$\lambda_\theta = r[\lambda_{v\theta}v_r/r - 2\lambda_{vr}(v_\theta + \dot{\theta}_E r)/r + \dot{\lambda}_{vr'}\sin\xi + \lambda_{vr'}\dot{\xi}\cos\xi - \dot{\lambda}_{v\theta'}\cos\xi + \lambda_{v\theta'}\dot{\xi}\sin\xi] \tag{34}$$

The reverse transformation taking ECR costates into a MCR frame is found by switching the E and M subscripts and switching r, θ, v_r, and v_θ with r', θ', $v_{r'}$, and $v_{\theta'}$ in Eqs. (30–34).

Although this transformation bypasses the need to satisfy the optimality conditions associated with the change of coordinate frame and state representations, it comes with practical tradeoffs. The numerical integration of the spacecraft's state around Mars in an Earth-referenced frame means that the position magnitude during the Martian spiral can be broken down into roughly two components of vastly different magnitudes. The first is the distance from Earth to Mars, which is on the order of $\sim 10^8$ km, and the second, the spacecraft's distance to Mars, which provides the fine detail of the spacecraft motion during the Martian spiral, is on the order of $\sim 10^3$ km at the terminal orbit. Similarly, the variation in the two spherical angles measured from Earth when the spacecraft is around Mars is very small. Because of these small variations in terms that require a high number of computational significant digits to span the vastly different scales involved with the integration of the spacecraft state in an Earth-referenced system when in close orbit around Mars, a discussion of the numerical accuracy of the Mars-to-Earth costate transformation is merited.

The software is written using double-precision FORTRAN coding standards, insuring the computer storage accuracy of each number to 16 digits. However, the numerical integration of both the states and costates is not an exact representation of the evolution of the governing differential equations. Rather, at each numerical integration time step, truncation error exists in addition to the computer round-off error beyond the 16th digit of each number in the calculation. The longer the integration, the larger the error that will accumulate. Because variable-step-size integration techniques are used, the truncation error inherent can be minimized by specifying a low error tolerance for each integration step. The low tolerance will drive the step sizes smaller when necessary to minimize truncation error to the proscribed tolerances.

However, there is a lower bound for achievable error tolerances as the cumulative computer round-off error for all the series of calculations grows during the integration. Cognizant of this source of error, when a trajectory is first run in Martian coordinates, its heliocentric terminal state is stored. The Mars-to-Earth costate transformation is then performed and the Martian trajectory is rerun based on the new ECR states and costates. The ECR states at the end of the integration are then transformed into heliocentric coordinates and compared with the heliocentric state found at the terminal point of the MCR trajectory. When comparing the ECR and MCR equivalent trajectories for shorter-duration spirals that start at moderate-to-high Martian orbits, the ECR solution converges to a position tolerance at least to the submeter level. As the Martian capture sequences are made increasingly more complex, the matching of the ECR and MCR trajectories still holds relatively well. These solutions match to the subkilometer level at the end of the integration. This close matching of the MCR capture spiral and equivalent ECR trajectory provides justification for the integration of the entire trajectory in the ECR frame, as performed in the following steps 5 and 6.

Step 5

The preceding four steps form the building blocks necessary to solve the full LEO–LMO missions solely in the ECR frame. For the unconstrained VSI case, there are eight unknowns and eight constraints. The initial and final polar angles of the spacecraft with respect to Earth and Mars are considered to be fixed as numerical sensitivity issues arise if these angles are free parameters. The initial guesses of four of the unknown costates come from the converged solution of step 3a and are the costates at t_0. The last four are the values returned from the transformation of the converged MCR costates of step 3b into their equivalent ECR costates at t_f. The eight constraints correspond to continuity of the four state variables and four costate variables at the patch point at which the forward and backward solutions meet. The constraints are evaluated in heliocentric space. Whereas previous works [4,5] analyzed these constraints and integrated the problem in astronomical canonical units, this work integrates the trajectories in actual metric measurements and evaluates the constraints as a percent error from the target value. The time of the patch point is important. Generally, it is chosen much closer to the final time than the initial time. However, it should never be set at any time after which the spacecraft has achieved zero energy with respect to Mars. If the patch point is too close to Mars, its gravity is too strong and can make convergence difficult. However, as discussed in step 6, setting the patch point far from the final time is not wise either.

Step 6

With the reality that numerically exact convergence is not likely for step 5, due to machine finite-word-length limitations and the complexity of the problem, the solution is refined one last step. Step 6 reduces the number of unknowns and constraints to four. The backward-spiral solution is removed and the four departure costates at t_0 from step 5 are run continuously to t_f at LMO with no patch point. The four targets are the four final state variables of the spacecraft at LMO. It is important for the patch point to not be too far from the final time, because any errors, however small, from step 5 will expand from the patch point until t_f. The further the patch point is from t_f, the greater the error there is for step 6 to correct. Step 6 allows these errors to be reduced through a final set of iterations on the boundary-value problem so that the spacecraft does achieve insertion into its final target orbit.

I_{sp} Constraints

The preceding six-step process is designed for unconstrained VSI engines in which the vehicle mass and power are decoupled from the problem via Eq. (17). Such trajectories that have the full control history of the spirals with the ability to freely vary the I_{sp} have not been presented previously. To directly compare with published research [4,5], I_{sp} constraints had to be considered, especially during the Earth escape. To accommodate such constraints, the costates from the unconstrained case are converted to the equivalent costates for a particular vehicle mass and power and the appropriate control limits are then added [3]. The six-step process is then slightly modified. Instead of steps 1a and 2a, maximum-energy spirals with a constant minimum I_{sp} are found in the ECI and ECR frames, which are in turn used in step 3a. For step 3a, once the spacecraft enters heliocentric space, the engine is allowed to vary between some minimum and maximum I_{sp} value. For the Mars captures, estimates need to be made for the final mass and mass costate to run the Mars-capture spirals backward for step 5, adding two unknowns to the boundary-value problem. Although these new unknowns add some

complexity to the problem compared with the unconstrained cases, these solutions are still easier to converge than the unconstrained VSI cases. The easier convergence behavior is due to the removal of the high-frequency oscillation of the acceleration magnitude (and I_{sp}) seen in the unconstrained cases during the Earth spiral. It is important to note that for all the missions presented that use I_{sp} constraints, the constraints are not overly strict and do not impose coast arcs on the solution. This type of trajectory with coast arcs is possible with constrained VSI engines, as shown for studies of Earth–Mars heliocentric-only transfers in [2]. However, such strict constraints (and the resulting coast arcs) are not imposed here, due to convergence difficulties that they would produce with the already-very-sensitive LEO-to-LMO problem posed.

Sample Mission Scenarios

The sample missions presented are used as a direct comparison with previously published works [4]. The orbits of Earth and Mars are assumed to be planar circular orbits with an initial phasing angle at which Mars is 36 deg ahead of the Earth. The initial orbit of the spacecraft around Earth is at an altitude of 320 km. The final orbit at Mars is set to be a circular orbit at 6 DU_M. The exhaust engine power is considered to be 6 MW and the initial mass is set at 525,000 kg. The total time of flight was set at 144 days. For initial guesses for the Earth-escape and Mars-capture spirals, spirals of 24 and 2 days, respectively, were used for steps 1 and 2. The I_{sp} is constrained to be 1000 s during the Earth escape and then is permitted to vary between 1000 and 35,000 s.

For the constrained mission, the final mass upon insertion to a circular orbit at 6 DU_M was 128,189 kg. The final mass for the same mission run in previously published research [4] was 127,331 kg, and so the new trajectory saves 858 kg of fuel, in comparison. However, there are numerous local optimal trajectories in the solution space, and they are very sensitive to the initial guess used for the capture sequence. This local optimal is 858 kg more efficient than the benchmark solution, but it should be noted that other local optimal solutions were found with poorer fuel efficiency than the previously published value for the final mass. A more in-depth discussion of local-vs-global optimal solutions is provided later. The same mission with an unconstrained engine has a final mass of 130,791 kg (2602 kg less fuel than the constant thrust case). A close-up of the Earth escape is shown in Fig. 3, and the capture to 6 DU_M is shown in Fig. 4.

The I_{sp} control history for the unconstrained case is shown in Fig. 5, and the I_{sp} control history for the constrained case is shown in Fig. 6. Notice the difference in the first portion of the two charts, in which the unconstrained case has a very detailed thrust history that oscillates with the position of the spacecraft with respect to the apogee and perigee of the instantaneous two-dimensional orbit. The constrained case greatly simplifies this portion of the mission, as seen in Fig. 6.

Initial and Final Polar Angles

For the preceding solutions, as mentioned earlier, the initial and final polar angles are fixed states. However, if these parameters are optimization variables, the corresponding targets are that the polar-angle costate must be zero in the ECR frame at t_0 and zero in the MCR frame at t_f. After scanning the solution space for the initial polar angle, it was found that the fuel usage was fairly insensitive to the initial polar angle with respect to Earth, because the fuel usage only changed by 33.5 kg over the 360 deg around the initial Earth orbit. This is a result of the long escape period, 24 days, over which the spacecraft makes enough orbits around Earth that changes to the initial angle can easily be adjusted for more than the period of the escape.

For the capture sequence to the 6-DU_M orbit, the solution is much more sensitive to the final polar angle. Depending on the targeted final polar angle around Mars, the solution had a range of fuel usages of 1125 kg. To find the actual optimal solution with respect to the final polar angle, the final polar angle was varied until the polar-angle costate in MCR coordinates was zero. The trajectories are calculated in ECR coordinates with ECR costates, and at the final time, the ECR to MCR costate transformation [as detailed in Eqs. (30–34), but reversed from the MCR-to-ECR case] is used to determine the final MCR polar-angle costate.

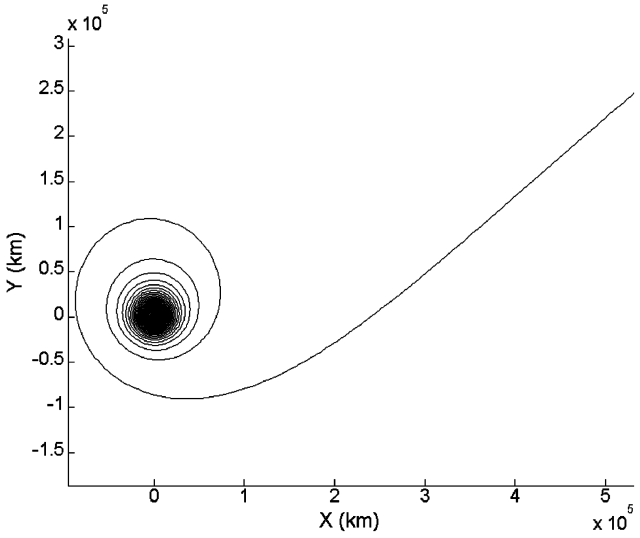

Fig. 3 ECR Earth-escape trajectory 0–24 days.

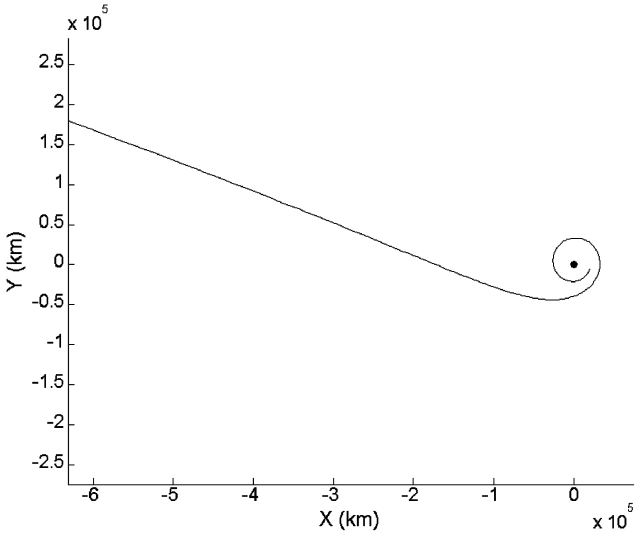

Fig. 4 MCR Mars-capture trajectory 139–144 days.

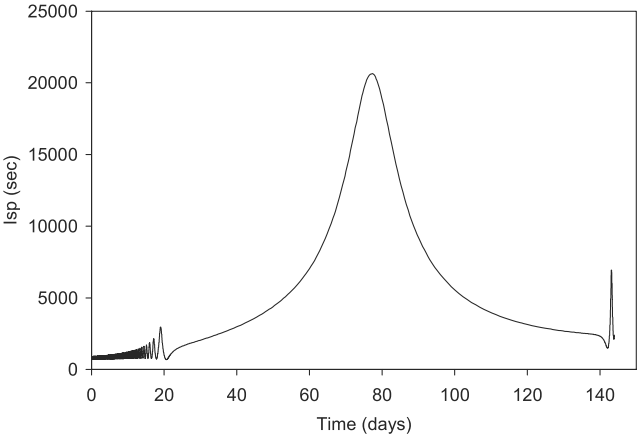

Fig. 5 I_{sp} vs time (unconstrained case).

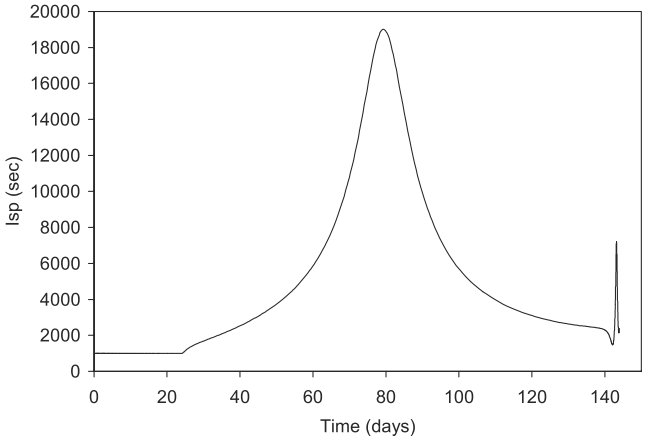

Fig. 6 I_{sp} vs time (constrained case).

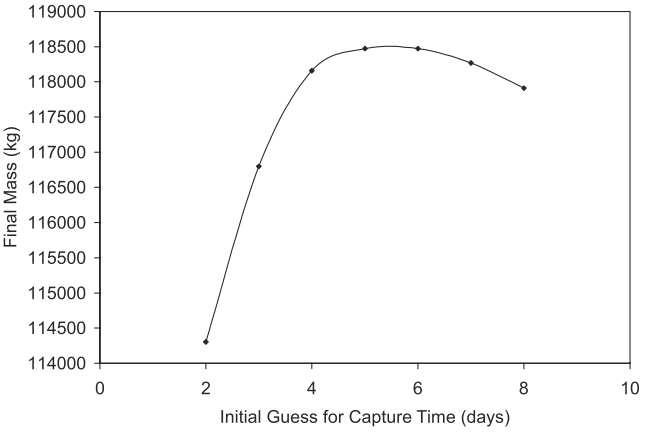

Fig. 7 Effect of spiral capture time on local optimal solutions.

Targeting Lower Capture Orbits and Local-Versus-Global Optimals

Previous work was only able to achieve 6-DU_M final orbits around Mars, but by using the methodology presented, more complex 1.77-DU_M circular Martian orbits are achieved. However, when exploring solutions that target lower Martian orbits, a limitation of the indirect method arose: the problem of local-vs-global optimal solutions. As expected, it was found that the solution space is filled with local optimal solutions. The most important parameter in determining which local optimal solution is found is the initial guess for the spiral escape and capture times used in steps 1–3. The final solutions found in steps 5 and 6 will converge to local optimal solutions in which the spiral escapes and captures take approximately the same amount of time and number of revolutions around the spiral bodies, as seen in the initial guess.

The local optimal solutions are affected by parameters such as the total time of flight, the initial Earth–Mars phasing, the engine and vehicle parameters, and the mission-defined initial and final orbits around Earth and Mars. A detailed study of the local optimal solution space as affected by the guess for the optimal capture time is shown for trajectories that terminate at a 1.77-DU_M Martian circular orbit. Figure 7 shows the final mass for a range of Mars-capture sequences. Each point on the curve corresponds to a converged local optimal trajectory to 1.77 DU_M, generated using the corresponding value along the x axis for the initial guess for the capture time used in steps 1–5. As a general rule, as the target orbit is lowered, longer spiral times will yield better fuel performance, as seen in Fig. 7. However, there is also an upper limit for the amount of time spent in the spiral, beyond which the fuel performance falls off. Figure 7 shows that the best local optimal solution with respect to the guess for capture time corresponds to an initial guess of six days for the Martian capture to the 1.77-DU_M circular orbit. The final mass for this solution is 118,473 kg. For the constrained case with a constant-I_{sp} escape spiral at 1000 s and a variable I_{sp} in the range of 1000–35,000 s for the rest of the mission, the final mass is 115,981 kg. Peak local optimal solutions such as the one found in Fig. 7 are loosely termed "global optimal solutions" for the rest of this study. The term *global* in no way implies that it has been theoretically shown to be globally optimal, but it has been experimentally shown to be better than all local optimal solutions found nearby with respect to the initial guess for the spiral times.

The behavior of this global optimal solution in comparison with the nearby local optimal solutions can be seen not only in the fuel dropoff on either side of six days in Fig. 7, it can also clearly be seen in the I_{sp} control histories. Figure 8 shows the I_{sp} profile for a local optimal solution found using eight days as the initial guess for the Mars-capture time. The mean value of the I_{sp} oscillation grows during the spiral capture. This indicates that the capture is taking too long with respect to the overall phasing of the mission. Basically, the spacecraft burned too hard through heliocentric space, arrived too quickly at Mars, and then had to wait because it arrived too soon. This waiting is achieved by using progressively higher I_{sp} to capture, but the fuel cost of arriving too soon cannot be totally recovered.

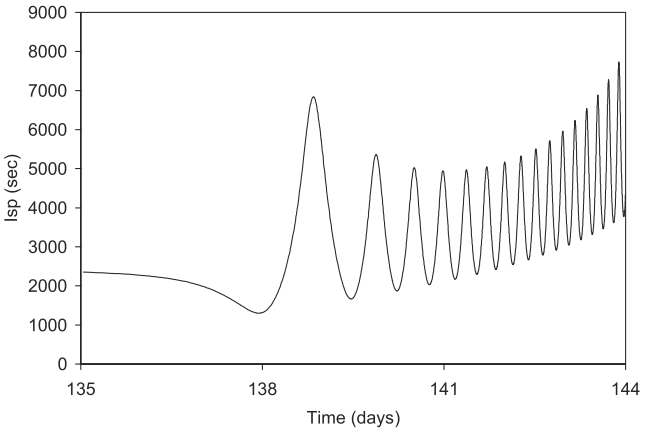

Fig. 8 I_{sp} history: initial guess for a capture time of eight days.

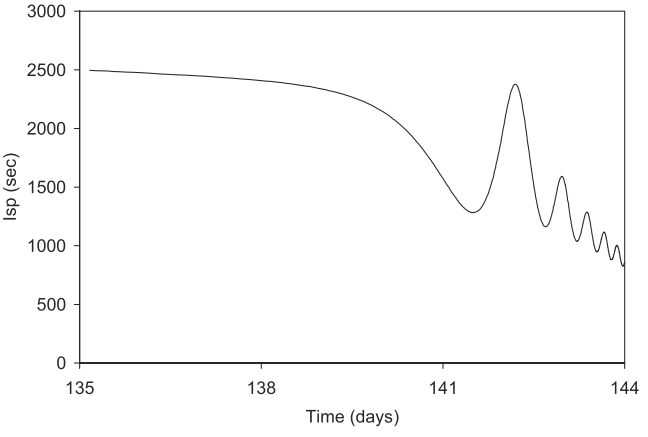

Fig. 9 I_{sp} history: initial guess for a capture time of two days.

Figure 9 shows the effect of arriving too late and having to execute a very fuel-intensive maneuver to achieve the final target orbit. In this case, the initial guess used to generate the local optimal solution is two days. The mean value of the I_{sp} oscillation decreases during the spiral capture to increase the thrust to achieve the more fuel-intensive capture.

The global optimal control history with respect to the capture time is shown in Fig. 10. Notice in this case that the mean value of the I_{sp} oscillation neither grows nor decays during the capture process. This indicates that this capture process is a global optimal solution in comparison with the local optimal solutions found for other capture times. This result was also found for Earth-escape spirals. Understanding this behavior allows an analyst to quickly identify if a

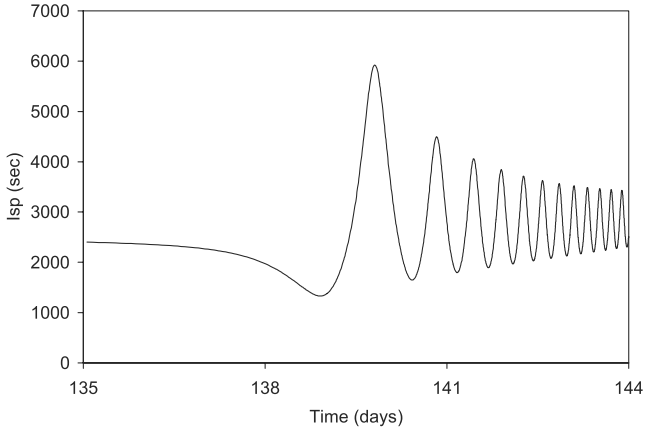

Fig. 10 I_{sp} history: initial guess for a capture time of six days.

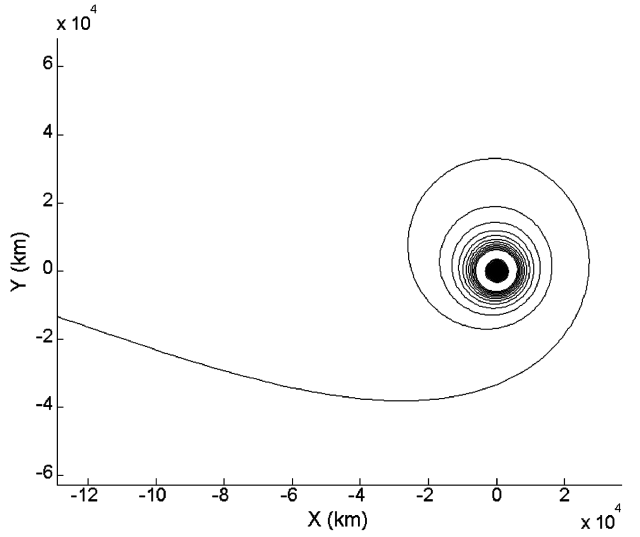

Fig. 11 MCR Mars-capture trajectory to 1.77 DU_M.

solution is a good local optimal solution or if further local optimal solutions should be generated until the expected control history is found. This is especially vital for these problems, due to the large number of local optimal solutions that exist. It also is an important factor for the increased performance in fuel and mission complexity compared with published benchmarks.

The other aspect of the control history, the thrust direction, is not plotted here. The thrust oscillates around the ECR velocity vector during the escape period of the mission and around the MCR antivelocity vector during the capture sequence. The actual capture trajectory to the final circular orbit of 1.77 DU_M around Mars is shown in Fig. 11 and is much more detailed than the previously lowest achievable captures to 6 DU_M, shown in Fig. 4.

Convergence Limits

Mission scenarios were also examined for final circular orbits of 1.32 DU_M (4500 km). Some locally optimal solutions were found that did achieve this final altitude but, due to numerical sensitivity issues, a full range of capture times was not converged. This limit of convergence is the practical boundary imposed by the error in the numerical integration due to the costate transformation for the Martian spiral that, when combined with the numerical integration error of the forward-integrated solution, is too large for the boundary-value solver to adjust meaningful numbers. Solutions were found for capture times up to, but not longer than, three days for the 1.32-DU_M case that, based on the behavior of the I_{sp} during capture, were probably not the global optimal solution. The mean value of the oscillation of the I_{sp} degraded in a fashion similar to that shown in Fig. 9. Additionally, the optimal capture time to the lower orbit should intuitively take longer than the 1.77-DU_M case, which took six days. The final mass for a three-day capture sequence was 110,454 kg.

Missions to 1.32 DU_M were also run with constraints on the I_{sp} (1000-s escape and 1000–35,000 s the rest of the way). The constraints, particularly during the Earth escape, simplify the control history and make solving the boundary-value problem less numerically sensitive. This simplification is shown because local optimal solutions for 1.32 DU_M were found for capture times as long as five days, whereas only three-day captures were numerically achievable with the unconstrained engine. The final mass is 111,805 kg, which is actually 1351 kg more than the unconstrained solution. This result is from the fact that the five-day Mars-capture sequence for the constrained case is closer to the global optimal for the Martian capture time than the three-day capture sequence found for the unconstrained case. This explains the better fuel performance for the constrained case. The global optimal solution for the unconstrained case, if it were numerically achievable, would be more fuel-efficient than the constrained global optimal.

Conclusions

A step-by-step process is detailed that allows the user to efficiently find fuel-optimal solutions using indirect optimization for interplanetary missions such as a low-Earth-orbit (LEO) to low-Mars-orbit (LMO) mission. The cornerstone of the process is the derivation of transformations that convert costates referenced to one coordinate frame to their equivalent set in another coordinate frame. This then permits the entire trajectory to be analyzed in a single coordinate frame. In turn, this allows the removal of optimality conditions that are required when solving such multiphase/multibody problems with multiple coordinate frames. These conditions are very numerically difficult to satisfy and avoiding them in the boundary-value problem is vital for converging difficult trajectories. The end result of the transformations yields highly accurate initial estimates of the spirals at Mars in Earth-referenced coordinates that can be integrated backward in time. Previously, for LEO-to-LMO transfers, the Martian captures had to be integrated forward, which is more difficult for generating multirevolution captures. Additionally, the long iterative process previously required to generate a single LEO-to-LMO trajectory is removed for a more efficient approach that can directly target a trajectory that satisfies the mission requirements from the first guess. The end result is that solutions are found with improved fuel performance, compared with previous studies. Trajectories are also found that increase the overall complexity (number of capture spirals and lower height of capture orbit) of the mission more than past endeavors have achieved.

Additionally, this process can accommodate solutions in which the vehicle specific impulse (I_{sp}) is either unconstrained or constrained. The unconstrained I_{sp} solutions have never been previously published, because the difficulties involved with finding the detailed control history for an unbounded I_{sp} mission, particularly during the long Earth-escape period, make solving the full LEO–LMO mission numerically sensitive. Building heavily on past research that focuses on accurately estimating the spirals, the full LEO–LMO mission with the unbounded I_{sp} solutions are solved. Solutions are also presented in which limits are considered on the I_{sp} values that are used for the comparisons with past published works. The previous lowest-achievable terminal orbit at Mars was six Mars radii (20,382 km), but solutions are now found as low as 1.32 to 1.77 Mars radii (4500–6000 km). The process discovered that the solution space is filled with local optimal solutions, particularly linked to the initial guess used for the escape and capture times. General rules are developed to quickly identify if a local optimal solution is likely a good local solution by examining the local optimal solution's I_{sp} history. Solutions with better performance have control histories that are visually distinct from the nearby poorer local optimal solutions. The local optimal solutions used for this comparison are generated by varying the estimates of the spiral times used in the initial guess.

Although this work is just for a two-dimensional model, the process developed can quickly give decent estimates of the fuel necessary for missions in an actual solar system and may provide good initial guesses for the costates and the planetary phasing for the three-dimensional problem. The transformation of the costates between coordinate frames could also be useful for problems such as gravity assists, and such problems may be explored in future work. Additionally, the theory behind this type of transformation could be quite useful when applied to Earth–moon transfers, especially for analysis in the restricted-three-body problem, in which the motion of the primaries is coplanar, as is the case in this work. The Earth–moon problems would also have significantly smaller problems due to scaling and numerical accuracy, as seen in the LEO-to-LMO problem. The next progression of this work will focus on developing the equations of motion and the appropriate transformations necessary to convert this two-dimensional step-by-step process into the equivalent three-dimensional process for LEO-to-LMO transfers.

Acknowledgments

The authors would like to express thanks for the support and funding for this research provided in part by the National Science Foundation Fellowship, the Thrust 2000 University of Texas Fellowship, and NASA grant NAG9-1441.

References

[1] Ranieri, C. L., and Ocampo, C. A., "Optimization of Roundtrip, Time-Constrained, Finite Burn Trajectories via an Indirect Method," *Journal of Guidance, Control, and Dynamics*, Vol. 28, No. 2, Mar.–Apr. 2005, pp. 306–314.

[2] Ranieri, C. L., and Ocampo, C. A., "Optimizing Finite Burn, Round-Trip Trajectories with I_{sp} Constraints and Mass Discontinuities," *Journal of Guidance, Control, and Dynamics*, Vol. 28, No. 4, July–Aug. 2005, pp. 775–781.

[3] Ranieri, C. L., and Ocampo, C. A., "Indirect Optimization of Spiral Trajectories," *Journal of Guidance, Control, and Dynamics*, Vol. 29, No. 6, Nov.–Dec. 2006, pp. 1360–1366. doi:10.2514/1.19539

[4] Vadali, S. R., Nah, R., Braden, E., and Johnson, I. L., Jr., "Fuel-Optimal Planar Earth–Mars Trajectories Using Low-Thrust Exhaust Modulated Propulsion," *Journal of Guidance, Control, and Dynamics*, Vol. 23, No. 3, May–June 2000, pp. 476–482.

[5] Vadali, S. R., Nah, R., and Braden, E., "Fuel-Optimal, Low-Thrust, Three-Dimensional Earth–Mars Trajectories," *Journal of Guidance, Control, and Dynamics*, Vol. 26, No. 6, Nov.–Dec. 2001, pp. 1100–1107.

[6] Pierson, Bion L., and Kluever, Craig, A., "Three-Stage Approach to Optimal Low-Thrust Earth–Moon Trajectories," *Journal of Guidance, Control, and Dynamics*, Vol. 17, No. 6, Nov.–Dec. 1994, pp. 1275–1282.

[7] Kluever, Craig A., and Pierson, Bion, L., "Optimal Low-Thrust Three-Dimensional Earth–Moon Trajectories," *Journal of Guidance, Control, and Dynamics*, Vol. 18, No. 4, July–Aug. 1995, pp. 830–837.

[8] Kluever, Craig A., and Pierson, Bion, L., "Optimal Low-Thrust Earth-Moon Trajectories Using Nuclear Electric Propulsion," *Journal of Guidance, Control, and Dynamics*, Vol. 20, No. 2, Mar.–Apr. 1997, pp. 239–245.

[9] Guelman, M., "Earth-to-Moon Transfer with a Limited Power Engine," *Journal of Guidance, Control, and Dynamics*, Vol. 18, No. 5, Sept.–Oct. 1995, pp. 1133–1138.

[10] La Mantia, M., and Casalino, L., "Indirect Optimization of Low Thrust Capture Trajectories," *Journal of Guidance, Control, and Dynamics*, Vol. 29, No. 4, July–Aug. 2006, pp. 1011–1014. doi:10.2514/1.18986

[11] Casalino, L., and Colasurdo, G., "Improved Edelbaum's Approach to Optimize LEO-GEO Low-Thrust Transfers," AIAA Paper 2004-5402, Aug. 2004.

[12] Tadashi Sakai, T., and Olds, J., "Development of a Multipurpose Low Thrust Interplanetary Trajectory Calculation Code," *Advances in the Astronautical Sciences*, Vol. 116, No. 3, Univelt, San Diego, CA, 2004, pp. 2597–2612; ; also American Astronautical Society Paper 03-667, Aug. 2003.

[13] Sakai, T., Olds, J., and Alemany, K., "Development of SAMURAI—Simulation and Animation Model Used for Rockets with Adjustable I_{sp}," *Advances in the Astronautical Sciences*, Vol. 120, No. 2, Univelt, San Diego, CA, 2005, pp. 1297–1316; ; also American Astronautical Society Paper 05-181, Jan. 2005.

[14] Sauer, C. G., Jr., "Optimization of Multiple Target Electric Propulsion Trajectories," AIAA Paper 73-205, Jan. 1973.

[15] Hull, D. G., *Optimal Control Theory for Applications*, Springer, New York, 2003, pp. 276–316.

[16] Lawden, D. F., *Optimal Trajectories for Space Navigation*, Butterworths, London, 1963, pp. 79–94.

[17] "Harwell Subroutine Library" [online database], http://www.cse.clrc.ac.uk/nag/hsl/ [retrieved 06 Dec. 2005].